


Formulation and Evaluation of PLGA Nanoparticulate-Based Microneedle System for Potential Treatment of Neurological Diseases

Baohua Li^{1,2,*}, Geng Lu^{1,2}, Wenbin Liu^{3,*}, Liqi Liao², Junfeng Ban^{1,2} , Zhufen Lu¹

¹Guangdong Provincial Key Laboratory of Advanced Drug Delivery, Guangdong Provincial Engineering Center of Topical Precise Drug Delivery System, Guangdong Pharmaceutical University, Guangzhou, People's Republic of China; ²The Innovation Team for Integrating Pharmacy with Entrepreneurship, Guangdong Pharmaceutical University, Guangzhou, People's Republic of China; ³Guangdong Provincial Key Laboratory of Pharmaceutical Bioactive Substances, Guangdong Pharmaceutical University, Guangzhou, People's Republic of China

*These authors contributed equally to this work

Correspondence: Junfeng Ban; Zhufen Lu, School of Pharmacy, Guangdong Pharmaceutical University, Guangzhou, Guangdong, 51006, People's Republic of China, Tel +86 20 39352362, Email banjunfeng@163.com; luzhufen@163.com

Introduction: The tight structure of the blood–brain barrier severely limits the level of drug therapy for central nervous system disorders. In this study, a novel composite delivery system combining nanocarrier and microneedle technology was prepared to explore the possibility of transdermal delivery of drugs to work in the brain.

Methods: Nanoparticle solutions containing paroxetine and rhodamine-B were prepared using PLGA as a carrier by the emulsification-solvent volatilization method. Then, they were mixed with hyaluronic acid and the PLGA nanoparticulate-based microneedle system (Rh-NPs-DMNs) was prepared by a multi-step decompression-free diffusion method. The particle size, zeta potential, and micromorphology of the nano solution were measured; the appearance, mechanical strength, dissolution properties, and puncture effect of the Rh-NPs-DMNs were evaluated; also, it was evaluated for in vivo live imaging properties and in vitro skin layer transport and distribution properties.

Results: The mean particle size of Rh-NPs was 96.25 ± 2.26 nm; zeta potential of 15.89 ± 1.97 mV; PDI of 0.120 ± 0.079 . Rh-NPs-DMNs had a high needle content of $96.11 \pm 1.27\%$ and a tip height of 651.23 ± 1.28 μ m, with excellent mechanical properties (fracture force of 299.78 ± 1.74 N). H&E skin tissue staining showed that Rh-NPs-DMNs produced micron-sized mechanical pores approximately 550 μ m deep immediately after drug administration, allowing for efficient circulation of the drug; and the results of in vivo imaging showed that Rh-B NPs DMNs had a faster transport rate than Rh-B DMNs, with strong fluorescent signals in both brain ($P < 0.01$) and hippocampus ($P < 0.05$) 48 h after drug administration.

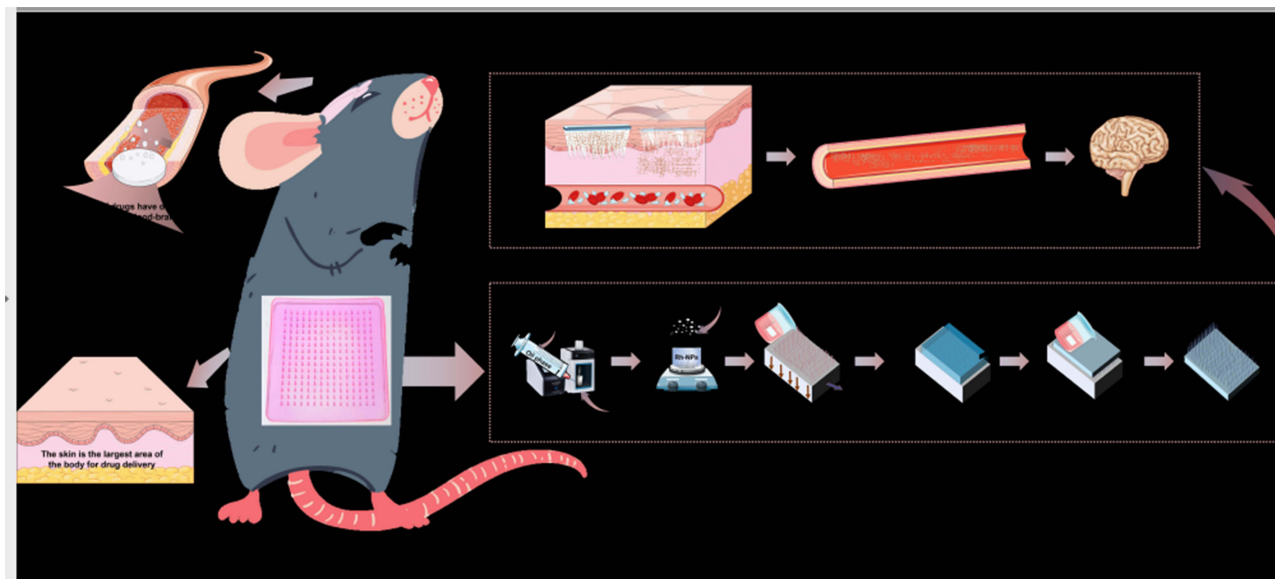
Conclusion: Nanoparticles can prolong blood circulation time and intracerebral retention time and have certain brain-targeting properties due to their excellent physical properties. The use of microneedle technology combined with nanocarriers provides new ideas for delivery systems for the treatment of central neurological diseases.

Keywords: soluble microneedle, PLGA nanoparticles, skin transfer, central nervous system

Introduction

Central nervous system (CNS) diseases have a high occurrence and disability rate, and the global number of patients with diseases is expected to increase in the future; therefore, it is important to intervene for preventing further deterioration of these patients. Although drug therapy has a huge potential in this field, its real clinical efficacy still needs to be amplified. The difficulty in the treatment of CNS disorders is the prevention of delivery of exogenous drugs to the brain tissue. Thus, how to safely and effectively transfer medications to the brain tissue is still a popular topic in academic research. Some of the reported invasive drug delivery techniques across the blood–brain barrier (BBB) comprise disrupting the tight junctions of BBB using ultrasound,^{1,2} magnetic resonance,³ or chemical means,⁴ intracranial drug delivery

Graphical Abstract



techniques based on direct drug delivery through the ventricles,⁵ intracerebral,⁶ or skull⁷ after craniotomy; convection-enhanced drug delivery techniques;⁸ and brain implantation techniques using polymer⁹ and microchips.¹⁰ The benefit of these invasive drug delivery strategies is that they can directly reach the brain tissue across BBB to apply the effects of the drug; however, they are prone to structural disruption of BBB, which may cause leakage of plasma proteins into the brain triggering chronic neurological changes such as neurotoxicity and neuroinflammatory reactions. Moreover, the use of mechanical devices on the brain may lead to a series of risks, including aggravation of intracranial infections, brain tissue damage, and thrombosis.

Transdermal drug delivery, as a non-invasive drug delivery system, has many advantages over traditional drug delivery methods (ie, injection and oral administration); moreover, it is very suitable for diseases requiring frequent or long-term treatment and is expected to replace various invasive drug delivery methods in the treatment of CNS and other diseases (eg, rheumatoid arthritis,¹¹ diabetes,¹² cardiac repairs,¹³ etc.). N-methyl-D-aspartic acid (NMDA) receptor dysfunction is closely related to neurological disorders; ketamine can be used for treating depression by inhibiting the NMDA receptor channel activity and participating in the regulation of synaptic transmission and plasticity signaling pathways, thus restoring synaptic damage in the cortical and hippocampal regions caused by chronic stress.¹⁴ Aaron¹⁵ prepared ketamine-loaded hydrogel-forming microneedle arrays and compared their differential pharmacokinetics with those of conventional intravenous administration. The results of their study showed that transdermal drug delivery could achieve ketamine plasma concentrations higher than the target concentration of $0.15\text{--}0.3\ \mu\text{g}\cdot\text{mL}^{-1}$ over 24 h, whereas intravenous drug delivery dropped to $0\ \mu\text{g}\cdot\text{mL}^{-1}$ at 2 h. Transdermal drug delivery is believed to be the novel treatment method for neuropsychiatric disorders. Pervaiz¹⁶ prepare novel paroxetine-loaded solid lipid nanoparticles (SLNs) based sustained-release transdermal patches, which could reduce side effects associated with high initial blood levels and fluctuating blood levels after oral administration; Also, it can reduce the frequency of administration, improve patient compliance, and establish a foundation for the study of transdermal delivery systems for PAX.

Based on the results of the above study, we experimentally prepared poly(lactic-co-glycolic acid) (PLGA) nanoparticles (NPs) loaded with paroxetine (selective serotonin reuptake inhibitor)¹⁷ and then loaded them into dissolving microneedles (DMNs) to improve their efficiency of drug delivery across BBB. We successfully constructed DMN arrays containing rhodamine B fluorescent probe NPs (Rh-NPs-DMNs) based on *in vivo* bioluminescence imaging and evaluated trans-BBB penetration using this delivery mode and the behavioral description of transdermal transport to

the brain. The results of the study confirm the possibility of its therapeutic effect in the brain by transdermal delivery and provide a basis for the foundation for the study of CNS drugs across the blood–brain barrier.

Materials and Methods

Materials

PDMS microneedle molds were provided by Microchip Pharmaceutical Technology Co., Ltd (Taizhou, China). Hyaluronic acid (HA-TLM 3–5), molecular weight ($M_w = 10,000$) was purchased from Bloomage Biotechnology Co., Ltd (Shandong, China). PLGA (50:50, $M_w = 10,000$) was manufactured at JUFK Biotechnology Co., Ltd. (Jinan, China). Paroxetine (Par) was purchased from Aladdin Biochemical Technology Co., Ltd (Shanghai, China). Rhodamine B was sourced from Damao Chemical Reagent Factory (Tianjin, China). Polyvinyl alcohol was bought from Kuraray International Trading Co., Ltd. (Shanghai, China). 2-hydroxypropyl- β -cyclodextrin was procured from Qianhui Biotechnology Co., Ltd. (Zibo, China). All other reagents and organic solvents were analytical reagents.

Balb/c-nu/nu mice, female, seven weeks old, weighing 16–18 g, were purchased from Guangdong Medical Experimental Animal Center, license number: SCXK (Guangdong) 2022–0002.

SD rats, female, four weeks old, weighing 100–300 g, purchased from Guangdong Medical Laboratory Animal Center, license No. SCXK (Guangdong) 2022–0002.

Construction of a Dissolvable Microneedle System

The preparation of dissolvable nanoparticle microneedles (Rh-NPs-DMNs) was based on the preparation of fluorescent rhodamine-loaded PLGA NPs using the emulsification-solvent volatilization method,¹⁸ followed by the multi-step decompression-free diffusion method.¹⁹ The preparation process comprised two steps. First, fluorescent dye (Rh, 2 mg) and paroxetine (200 mg) were added to the oil phase, and PLGA (LA:GA = 50:50, $M_w = 10,000$, 50 mg) was dissolved in 20 mL of dichloromethane: acetone (3:1) solvent mixture which served as the organic phase; the aqueous phase was made up of 1.5% 2-hydroxypropyl- β -cyclodextrin and 2% polyvinyl alcohol in 20 mL of the aqueous solution, and the pH was adjusted to 3 using dilute hydrochloric acid. Then, the organic phase was gradually injected into the aqueous phase in an ice-water bath for ultrasonic emulsification (JY88-IN, Scientific Biotechnology Ltd, People's Republic of China, variable amplitude rod: 6 mm, power: 270 W, interval: 3 s) for 30 min. Finally, Rh-NPs were obtained via magnetic stirring at 300 rpm until the organic phase was completely volatilized, followed by making up the volume of the mixture to 20 mL using deionized water. The second step was to add HA (HA-TLM 3–5, $M_w = 10,000$) to the prepared Rh-NPs, and the ratio was controlled at 1:10 (m/v); this was stirred at low speed until the solution was completely swollen. Then, the sample was centrifuged at 5000 rpm for 5 min. Next, the supernatant was taken out, poured into PDMS microneedle molds, and spread evenly; then, it was transferred to a vacuum drying oven (DP33C, Yamato Co., Japan) and degassed to -0.08 Mpa for approximately 30 min, followed by removal of the matrix solution. After removing the matrix solution containing air bubbles, the above process was repeated until the matrix material filled the pinholes of the mold; finally, the matrix solution was added so that the backing layer was filled, rested at 25 °C for 20–30 min, then placed at 40 °C (DKN612C, Yamato Co., Japan), cured for about 8 h, and demoulded.

To demonstrate the effect of NPs on brain-targeted delivery, the fluorescent rhodamine-loaded hyaluronic acid-based microneedle system (Rh-DMNs) was prepared for comparison with Rh-NPs-DMNs. Rh-DMNs were prepared by directly adding the same amount of rhodamine as above to the aqueous solution of HA (10% w/v) and stirring uniformly and preparing the microneedle system using the multi-step decompression-free diffusion method.

Evaluation of the Properties of Rh-NPs-DMNs

Good formability and adequate mechanical strength are important factors for ensuring that the microneedle does not bend or break during percutaneous delivery, thus ensuring puncture efficiency.

Film Thickness and Flatness

To examine the mechanical strength, capability to cross the stratum corneum barrier, and ensure effective drug delivery of the microneedle system, the degree of film formation, flatness, and the presence of air bubbles in the backing layer of

the microneedle system are the primary factors that should be assessed. Rh-NPs-DMNs were placed on slides and observed for flatness and film formation using the stereo microscope (S6D, Leica Co., Germany).

The microneedles were similarly placed under the polarizing microscope (TrueChrome II cx41*/Olympus Co., JAPAN) to observe the tip-forming results layer by layer, and the needle tip-forming effect (N_{eff}) was calculated according to the following equation (1).

$$N_{eff} = \frac{T_n - D_n}{T_n} \times 100\% \quad (1)$$

Where T_n is the total number of needles and D_n is the defective-shaped needles.

Scanning Electron Microscopy

Scanning electron microscopy (Gemini SEM 300, ZEISS Co., Germany) was used to observe the appearance of the microneedles and the surface structure of the needles; the samples were subjected to gold spraying (platinum as the target material) for 20s on an ion sputtering instrument (JFC-1600, JEOL, JAPAN) before being placed in a low vacuum thermal field emission scanner (10 kV) for observation.

Determination of Nanoparticle Properties

To assess whether NPs can significantly improve the efficiency of transport across BBB, the particle size, surface charge, encapsulation efficiency (EE), and drug loading (DL) are the critical factors that should be analyzed.²⁰ Rh-NPs were diluted in appropriate amounts, controlled at $(25 \pm 1)^\circ\text{C}$, and determined by Delsa Nano C laser particle sizer (Beckman Coulter Inc., CA, USA) to determine the particle size distribution range, polymer dispersity index (PDI), and Zeta potential of the NPs in the system. Additionally, the morphologic and size characteristics of the NPs in the system were further observed via transmission electron microscopy (JEM-1400, JEOL, JAPAN). Rh-NPs were appropriately diluted in distilled water and then dropped onto the copper mesh with a carbon film stained with 2% phosphotungstic acid solution for 10 min for observation after the mesh was dried. The encapsulation efficiency and drug loading of the nanoparticle solution were determined by ultrafiltration-centrifugation method,²¹ by taking an appropriate amount of nano-solution in a centrifuge tube with 1000 rpm for 10 min to obtain the supernatant of nanoparticles and little dissolved drug, and then transferring the upper liquid to an ultrafiltration tube (with a retention molecular weight of 3 kd) and centrifuging it at 15,000 rpm for 30 min at 4°C to separate the dissolved drug from the nanoparticles. The dissolved drug was separated from the nanoparticles. The drug content in the nanoparticles was determined by HPLC, and the EE and DL of the nanoparticle system were calculated according to the following equations.

$$EE(\%) = \frac{C_1 - C_2}{C_0} \times 100\%$$

$$DL(\%) = \frac{(C_1 - C_2)V}{M} \times 100\%$$

where C_0 is the initial concentration of drug, $\mu\text{g}\cdot\text{mL}^{-1}$; C_1 is the concentration of drug in the supernatant after low-speed centrifugation, $\mu\text{g}\cdot\text{mL}^{-1}$; C_2 is the concentration of drug in the filtrate in the ultrafiltration tube, $\mu\text{g}\cdot\text{mL}^{-1}$; V is the volume of nanoparticle solution, mL; M is the total amount of drug and PLGA in the nanoparticle solution, mg.

Evaluating the Mechanical Strength of Rh-NPs-DMNs

The two types of microneedles were assessed using the texture analyzer (TA-XT plus, Stable Micro System Inc., CA, UK) to establish mechanical strength. A P/2 probe (diameter of approximately 2 mm) was selected and set to move down at a speed of $0.01 \text{ mm}\cdot\text{s}^{-1}$. When the probe contacted the tip of the needle and started to apply pressure and reached a trigger force of 0.05 N, the pressure sensor began to record the change in pressure until the compression deformation reached 90%, the probe stops pressing down and remains until the microneedle patch crushes before ending the measurement. During the measurement, the texture analyzer records the change of probe pressure with time and plots the time–force relationship with time as the x-axis and probe pressure as the y-axis. And the probe pressure

corresponding to the inflection point of the mechanical strength curve was used as the fracture force of the microneedle patch, and the magnitude of this value was used to assess the mechanical strength of the microneedle.

Evaluation of Transdermal Permeation of Microneedle System

The skin penetration of the two microneedles was simulated using Parafilm[®] M film,²² and the efficiency of the microneedles in reaching different depths was assessed by analyzing the depth of penetration of the microneedles into various layers of the film. Eight layers of Parafilm[®] M film (approximately 127 μm thickness each) were flattened and stacked on polystyrene foam templates (approximately 5 mm thickness), while the microneedle was placed over the stacked films and held for approximately 30s by finger pressure. Finally, the Parafilm films were separated layer by layer, and the number of micropores generated after microneedle action on each layer was recorded, the penetration efficiency (P_{eff}) was calculated according to equation (2), and the x-y axis was plotted with the penetration efficiency as the vertical coordinate and the depth of penetration as the horizontal coordinate to assess the depth of microneedle drug delivery reaching the skin.

$$P_{\text{eff}} = \frac{N_m}{T_n} \times 100\% \quad (2)$$

where P_{eff} refers to the penetration efficiency, N_m refers to the number of micropores on the membrane, and T_n is the total number of needles on the microneedle patch.

In vivo Evaluation of Rh-NPs-DMNs Transport Behavior Using Fluorescence Imaging

To further evaluate the influence of the properties of nanoparticle-laden microneedles on drug transport and distribution in vivo after transdermal administration of microneedles. In vivo imaging technology (VISQUE In vivo Smart-LF, Biotimes Technology Inc., CA, CHINA) was used to visualize the changes in fluorescence intensity at the administration site over time and the fluorescence distribution of NPs in the organ and tissues after the administration of the two microneedles. To avoid the effect of animal hair on the fluorescence signal, the experiments were conducted in adult healthy Balb/c-nu/nu mice, and the animals were randomly divided into two groups. First, after preparing 1% sodium pentobarbital, the mice were anesthetized by intraperitoneal injection of sodium pentobarbital (1%) at 5 $\text{mg}\cdot\text{kg}^{-1}$ body weight and the mice were fixed on a plate to ensure that they were lying flat throughout the test. Then, to dynamically observe the drug penetration behavior in the skin, Rh-DMNs, and Rh-NPs-DMNs were pressed into the abdominal skin of nude mice for 10 min (the needle tips were completely dissolved) and the treated mice were placed into the live imaging chamber for imaging (green light source, excitation light: 530–570 nm, emission light: 575–640 nm, the field of view: 15×15 , exposure time: 500 ms, aperture: F1.8) at preset time points (0 min, 10 min, 30 min, 60 min, 2 h, 3 h, 4 h, 6 h, 9 h, 12 h, 24 h, and 48 h). To further observe the retention of the drug in the body, the animals were injected with an overdose of pentobarbital sodium 48 h after administration of the nanoparticle-laden or nanoparticle-free microneedle system and then dissected to explore the accumulation of fluorescence in the brain, heart, liver, spleen, lung, and kidney, and the fluorescence signal was quantified using the IVIS system.

Ex vivo Evaluation of Transdermal Transport of Microneedles

It is important for the dissolution rate of Rh-DMNs to correlate with drug release patterns, and to understand the dissolution profile of the Rh-DMN matrix when it is placed in contact with the skin. The abdominal skin of Sprague-Dawley rats used for the study should be depilated with subcutaneous fat and connective tissue removed²³ was used to investigate the dissolution rate of the microneedle tips. After washing rat skin with physiological saline, the skin surface was rubbed dry and placed flat on the platform of the Texture analyzer. The two types of microneedles were attached to the probe (P/50) of the texture analyzer with the tip perpendicular to the abdominal skin; the probe was set to move toward the platform at a speed of 2 $\text{mm}\cdot\text{s}^{-1}$. When the trigger pressure of 0.05 N was reached, the probe changed its speed to 0.5 $\text{mm}\cdot\text{s}^{-1}$ and continued to move downward. Once the pressure increased to 50 N, the probe was held for 5 s and then moved in the opposite direction. The microneedles retained on the skin were removed at 5s, 10s, 30s, 60s, 2

min, 5 min, and 10 min, respectively, and the swelling and dissolution of the microneedles were observed using a texture analyzer.

Ex vivo Skin Permeation Studies

The stratum corneum barrier is the primary factor that affects the transdermal delivery of drugs. A Franz transdermal diffusion tester (TK-12B, Testing Instrument Co., CHINA) was used to assess the drug transport and distribution in the skin layer using the abdominal skin of SD rats (female, 80–100 g, 4 weeks) with subcutaneous fat and connective tissue removed as the medium. The isolated skin was placed between the donor and receptor compartments, with the stratum corneum facing the donor compartments and the skin tissue facing the receptor compartments. The receiving solution is 18 mL of PBS (pH 5.2, typical pH of healthy non-diseased skin is around 4.0–6.0),²⁴ ensure that it is in complete contact with the skin (area of 3.14 cm²), and with the application of approximately 50 N force on the surface of the stratum corneum to cause the microneedle to pierce the abdominal skin of SD rats. The temperature was maintained at 32°C ± 0.5°C with a rotation speed of 300 r·min⁻¹ to simulate the physiological conditions of blood and tissue fluid circulation under human skin. The skin of the microneedle administration site was removed at 10 min, 1 h, 4 h, 8 h, and 12 h, respectively, and the skin surface was washed with physiological saline until there was no drug residue, fixed with 4% paraformaldehyde overnight, rinsed with PBS, and immersed in 20% sucrose solution until the tissue mass was immediately extracted after observation of sinking and frozen sections were processed according to a previously described method.²⁵ The laser confocal microscope (STELLARIS 5, Leica Co., Germany) was used to visualize the changes in fluorescence intensity and the depth of microneedle distribution.

In vivo Evaluation of Transdermal Transport Mechanism

Microneedle penetration depth in the skin and changes in microneedle orifices at different time points were analyzed by hematoxylin–eosin (H&E) staining in the normal control group (only depilatory treatment) and SD rats after administration of Rh-NPs-DMNs versus Rh-DMNs, respectively. The microneedle patch was pressed onto the abdominal skin of SD rats and held for about 30s. The microneedle was fixed on the skin with medical tape, and the administered animals were executed by intraperitoneal injection of sodium pentobarbital at 10 min, 12 h, and 24 h, respectively, after which the administered skin tissue was dissected.²⁶ The relevant skin tissues were fixed in 4% paraformaldehyde tissue for 24 h, then the tissues were gradually dehydrated using ethanol as a dehydrating agent and xylene (I, II, III, 20 min each) to make the tissues transparent. The transparent tissues were removed and placed sequentially in wax cylinders (I, II, III, IV, each for 30 min) for wax immersion, and finally, after sectioning, spreading, baking, H&E staining, and sealing, the differences in skin structure before and after microneedle administration were examined using Aperio ImageScope x64c[®].

In vivo Evaluation of the Healing Potential of Microneedle System

The microporous channel mechanism confirmed by microneedles can effectively overcome the stratum corneum barrier, diffuse CNS drugs to the deeper layers of the skin, and deliver them to the target site by the penetration and diffusion of tissue fluid. The abdominal skin of healthy Balb/c-nu/nu mice (female, 16–18 g, 7 weeks) was chosen for observing the healing of the microneedle in the skin orifice after drug administration. The microneedle was pressed perpendicular to the skin surface for 3 min; then, after removing the microneedle patch, the status of the microneedle site was continuously observed at 0 min, 2 min, 5 min, 10 min, and 15 min, and the time required for the skin to completely return to the pre-puncture state was noted.

Data Analysis and Statistics

All data were expressed as Mean ± S.D. and were statistically analyzed using Origin 2018 64Bit and GraphPad Prism 9.0. One-way analysis of variance was used for statistical analysis to evaluate the significance of statistical differences in experimental data. **P* < 0.05 was considered as a statistical difference.

Results

Evaluation of Rh-NPs-DMNs Properties

Drug delivery based on NPs is one of the new treatment methods for CNS diseases. However, to assess the characteristics of NPs microneedles for effective drug delivery across BBB to the brain after transdermal administration, the NPs microneedles should be prepared based on the fluorescent dye rhodamine-B (Rh) loaded into them as fluorescent probes. Under the stereo microscope, Rh-NPs-DMNs and Rh-DMNs made using the multi-step decompression-free-diffusion method were prepared as neatly arranged, unbroken, 15×15 quadrilateral conical microneedle arrays with tip distances of $800.91 \pm 1.98 \mu\text{m}$ and $802.35 \pm 1.64 \mu\text{m}$, respectively (Figure 1A, $n = 12$). The needle tip forming effect (N_{eff}) of Rh-NPs-DMNs and Rh-DMNs was observed using the polarizing microscope and recorded to be $96.11\% \pm 1.27\%$ and $92.36\% \pm 0.97\%$, respectively (both $>85\%$). Using IS Capture[®] application, the needle length of Rh-NPs-DMNs and Rh-DMNs was measured to be $651.23 \pm 1.28 \mu\text{m}$ and $651.71 \pm 1.21 \mu\text{m}$, respectively (Figure 1B, $n = 12$). Scanning electron microscopy revealed that the connection between the microneedle body and backing layer was tight, there were no hollows or air bubbles in the microneedles (Figure 1C and D), and the tip of the needle had a multilayer quadrilateral cone structure with a top area of less than $300 \mu\text{m}^2$, having enough tip sharpness to puncture the skin.

The size and surface charge of NPs is important elements for improving the efficiency of transport across BBB.²⁰ NPs with a particle size of less than 200 nm and a PDI of less than 0.2 can break BBB, providing a promising innovative approach for solving the challenge of drug entry into the brain.²⁷ The stability of the system is affected by different PLGA polymerization ratios; thus, those that affect the range of NPs size distribution were investigated in the experiment. Figure 2A shows that at the same Mw, the particle size distribution of the system tends to decrease with an increase in the proportion of hydrophilic polymer polyglycolic acid in the copolymerization ratio. At the copolymerization ratio of 50/50, the system has the smallest distribution range and the average particle size is less than 100 nm so that NPs with a narrow distribution of the system determine the contact area and contact mode between the nanomaterial and the cell membrane to a certain extent, which is the key to affect its transport process in vivo. Eventually, NPs with a particle size of approximately 100 nm were optimized for the preparation process via research experiments, and the NPs in this size range were able to cross the stratum corneum barrier through passive diffusion.²⁸

Following the preferred NPs process, Rh-NPs were prepared using fluorescent pink emulsion, which could yield the “Tyndall effect” (Figure 2B); the system was homogeneous and stable. The laser particle sizer revealed that it was

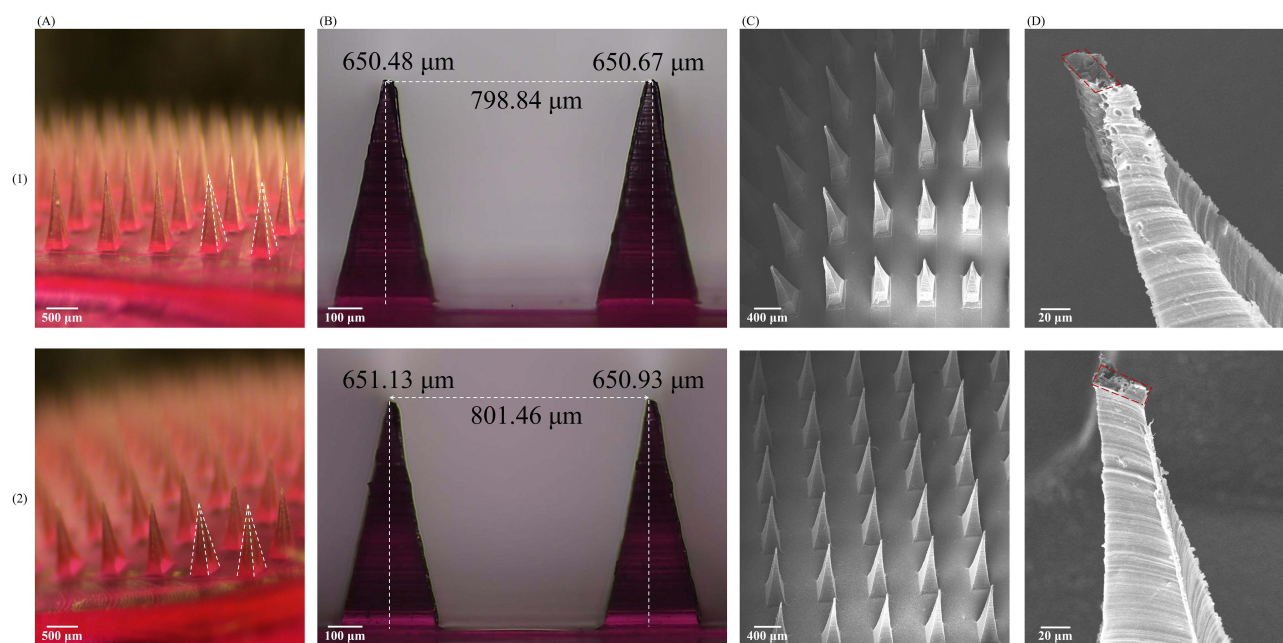


Figure 1 Characterization of fluorescent probes. ((A) SM (1.25×, Scale bars = 500 μm); (B) PM (4×, Scale bars = 100 μm); (C) SEM (25×, Scale bars = 400 μm); (D) SEM (500×, Scale bars = 20 μm) (1: Rh-NPs-DMNs; 2: Rh-DMNs).

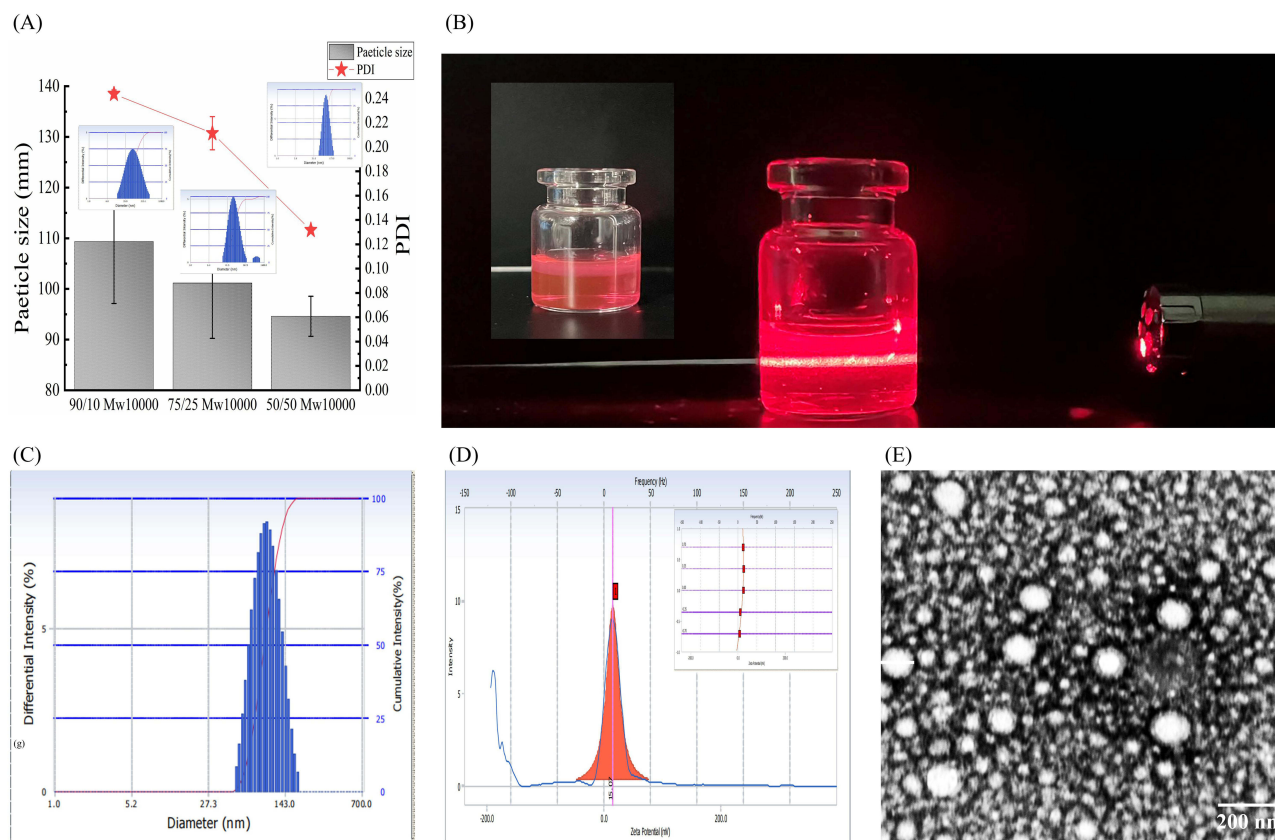


Figure 2 Characterization of Rh-NPs. ((A) variation in particle size; (B) appearance properties; (C) particle size distribution; (D) zeta potential; (E) TEM (28 \times , Scale bars = 200 nm)).

a monodisperse system with an average particle size of 96.25 ± 2.26 nm (Figure 2C, $n = 12$, the same below), zeta potential of 15.89 ± 1.97 mV (Figure 2D), and PDI of 0.120 ± 0.079 . Transmission electron microscopy revealed that NPs were spherical and uniformly dispersed (Figure 2E), and the calculated particle size (97.70 ± 8.02 nm) was similar to that determined by the laser particle sizer method. In addition, the encapsulation efficiency of the nano-solution was measured to be $87.40 \pm 3.86\%$ and the drug loading to be $2.66 \pm 0.66\%$.

Mechanical Performance Evaluation

Chi et al²⁹ used HA (Mw = 10,000) to prepare Rh-DMNs and reported that a fracture force of 0.21 N per needle tip can produce adequate puncture efficiency. Figure 3A shows that when the probe is displaced to the tip length of Rh-NPs-DMNs at 650 μ m, the fracture force of the tip is 2.75 ± 0.03 N ($n = 12$, approximately four needles), which is 1.8 times higher than that of Rh-DMNs, generating a force sufficient to overcome the elastic barrier of the skin. The reason for this may be related to the fact that the 2-HP- β -CD-based PLGA system forms hydrogen bonding with HA,³⁰ restraining the migration of molecular chains and tightening the structure, thus increasing the mechanical strength of this composite. The maximum mechanical strength value of Rh-NPs-DMNs can reach 299.78 ± 1.74 N ($n = 12$; Figure 3B) when the maximum compression distance is approximately 2 mm, whereas that of Rh-DMNs is only 196.62 ± 1.71 N ($n = 12$). Rh-NPs-DMNs prepared by combining HA with PLGA NPs as a matrix material can effectively improve the mechanical properties of the microneedle system and guarantee the effective delivery of drugs.

The degree of penetration of the microneedle system into the parafilm was almost 100% when the microneedle was inserted into less than three layers (Figure 3C), and quadrilateral shapes were seen at the bottom cross-section of the microneedle tip in the first layer (Figure 3D). After more than four layers, it could only form an impression in the 4th and 5th layers, and the penetration efficiency of complete penetration decreased to approximately 60% in the 4th layer and

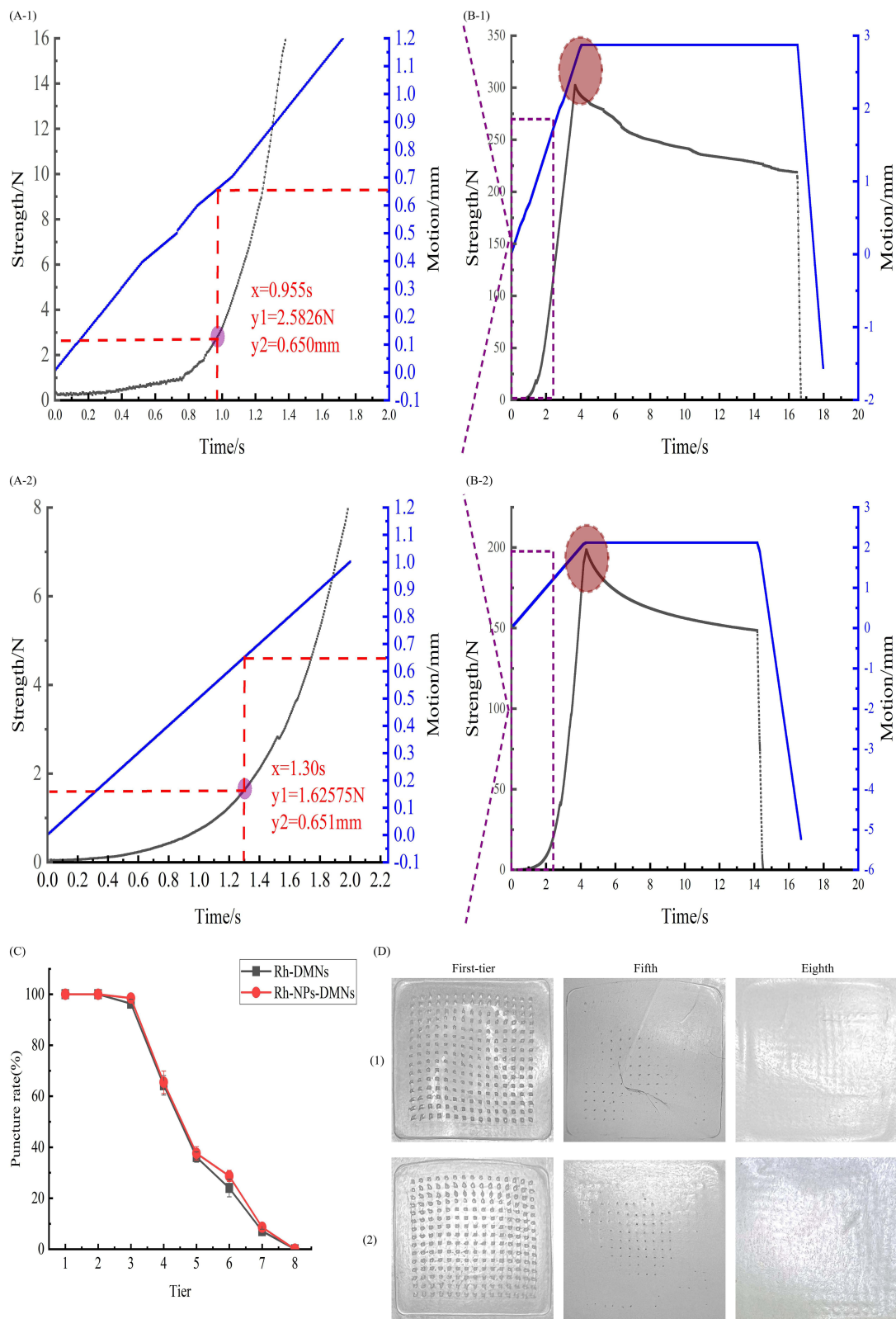


Figure 3 Characterization of Rh-NPs-DMNs (1) and Rh-DMNs (2). ((A) local fracture force at the tip; (B) overall fracture force; (C) the trend of puncture (points indicate Mean \pm S.D.) (n = 3 independent experiments with three technical replicates); (D) perforation changes in each layer of membrane)(1: Rh-NPs-DMNs; 2: Rh-DMNs).

approximately 40% in the 5th layer. When it reached the 6th layer, the penetration efficiency decreased to approximately 20% although a more obvious impression could be formed at the stress site when the depth exceeded 650 μm . The penetration rate in the 8th layer was 0%, with almost no impression of microneedle penetration. Using a polystyrene foam template to simulate the elastic space of skin,³¹ it was predicted that microneedle drug delivery could reach a certain depth of the skin, however, without touching the subcutaneous dermis (ie, the eighth layer of the Parafilm film), which is filled with blood vessels and nerves for approximately 1000 μm . In summary, the microneedles prepared herein not only have a good appearance and formability but also sufficient mechanical strength to ensure that the microneedles do not fracture after penetration into the skin due to skin peristalsis and external driving effects. The combination of NPs and microneedles increases the strength and stiffness of the microneedles, thus guaranteeing that no fracture or flexion damage occurs when the microneedles are inserted and enhancing the efficiency of transdermal delivery.

Transdermal Delivery Efficiency Across BBB

The skin fluorescence intensity detected through near-infrared in vivo imaging was positively correlated with the concentration of fluorescent drug (Rh).³² As shown in Figure 4A, the fluorescent intensity of the Rh-NPs-DMNs group showed an increasing trend from 1.81×10^{15} [p/s/cm²/sr]/[$\mu\text{W}/\text{cm}^2$] to 2.48×10^{15} [p/s/cm²/sr]/[$\mu\text{W}/\text{cm}^2$] during

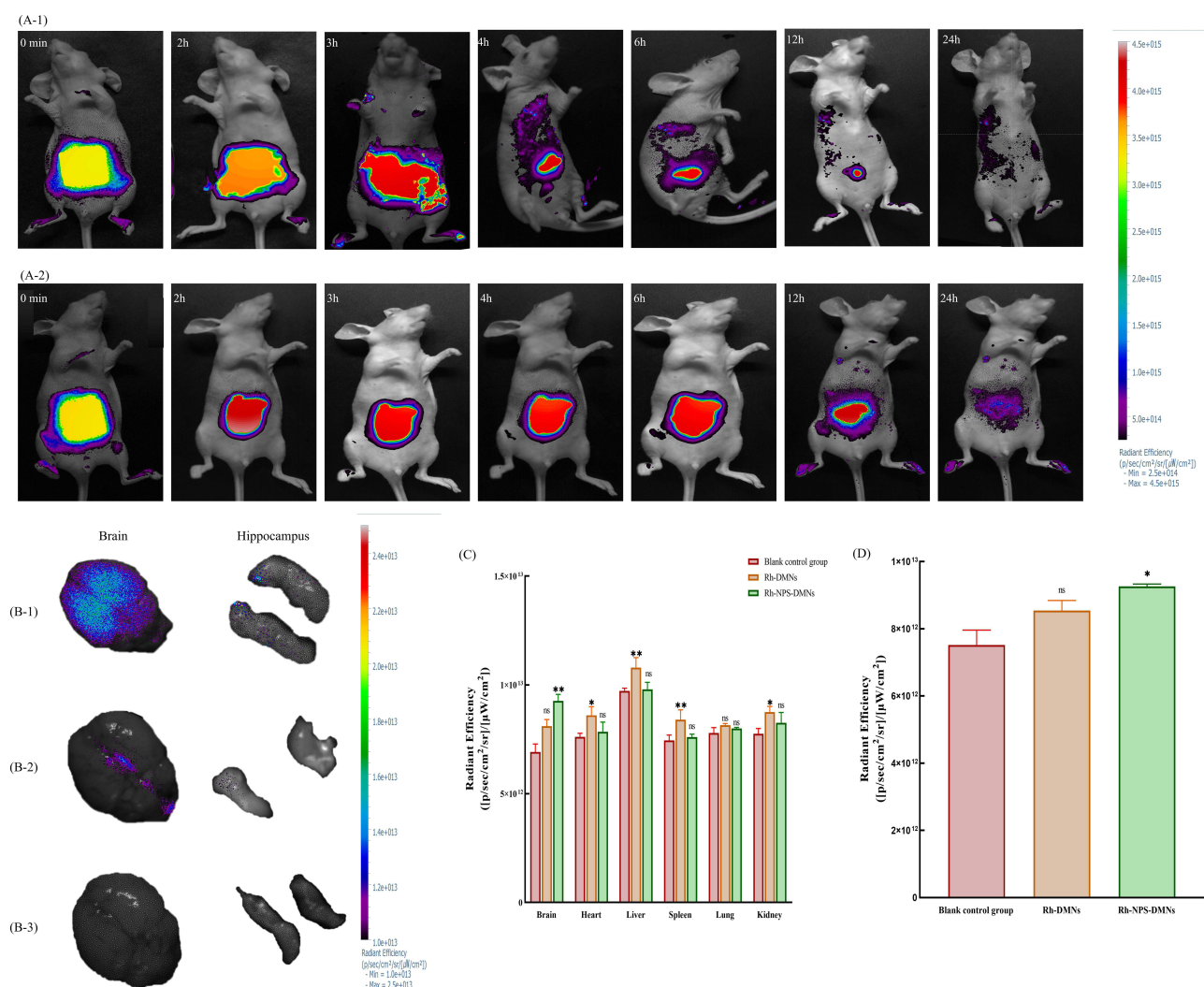


Figure 4 (A) Fluorescence signal intensity distribution at different time points; (B) Fluorescence signal intensity distribution of major organs; (C) Organ collection of fluorescent signals; (D) Hippocampus collection of fluorescent signals. (Bars indicate mean \pm S.D.) (n = 3 independent experiments with three technical replicates) (* $P < 0.05$; * $P < 0.05$, ** $P < 0.01$) (1: Rh-NPs-DMNs; 2: Rh-DMNs; 3: blank controls).

0–3 h, which was due to the embedded skin needle tip layer in the tissue fluid gradual dissolution and diffusion under the action of the micro-needle patch with the simultaneous release of drug at this stage. Subsequently, the fluorescence intensity showed a decreasing linear trend. The reason for this might be the fact that the drug slowly diffused into the dermis and subcutaneous tissues and was then absorbed through the capillary network whereby it entered the body circulation, with almost no fluorescence signal at 48 h ((5.85397×10^{13}) [p/s/cm²/sr]/[μW/cm²]); there were no significant differences compared with the blank group. In contrast, the fluorescence intensity of the Rh-DMNs group showed a sudden release (from (1.17×10^{15}) [p/s/cm²/sr]/[μW/cm²] to (2.40×10^{15}) [p/s/cm²/sr]/[μW/cm²]) within 4 h after drug administration; it was still significantly higher than that of the Rh-NPs-DMNs group at 12 h (** $P < 0.01$), suggesting that the drug of this system penetrated the stratum corneum and accumulated in the active epidermis and the amount of drug entering the dermis was relatively limited. Thus, Rh-NPs could enhance the ability of drug penetration through biological membranes and could diffuse through the basement membrane of the epidermis to the dermis, resulting in an effective increase in dermal transit rate.

As seen in Figure 4C, compared with the blank group, the brain, heart, liver, spleen, lung, and kidneys of the Rh-DMNs group showed some degree of fluorescence. The presence of strong fluorescence in the liver and spleen in the Rh-DMNs group ($*P < 0.01$) can be explained by the liver being the main organ of metabolism, which tends to allow the accumulation of drugs there, as well as the fact that the administration site was located in the abdominal skin of mice, which was thin enough to allow the microneedle to pass through the skin directly into the surface layer of liver tissue. The spleen is the largest lymphatic organ in the body; approximately 90% of the blood circulation of the body flows through the spleen. This proves that microneedle drug delivery effectively delivers active ingredients to the deeper layers of the skin and also passes them through the association of lymphatic circulation and blood circulation, allowing them to be delivered to the lesion site. Subsequently, the results of the dissection of brain tissues performed to isolate the hippocampus in close order are shown in Figure 4B and D; the Rh-NPs-DMNs group had a stronger fluorescence in the brain and hippocampus than the blank group. There was no significant difference in other organs of the Rh-NPs-DMNs group compared with the blank group ($^{ns}P > 0.05$), and the reason for this phenomenon may be that PLGA is a biodegradable and biocompatible material with good stability, which can increase the intracerebral concentration of the drug and simultaneously extend the retention time of the drug in the brain with brain targeting.²⁷

Mechanism of Transdermal Delivery Across BBB

To elucidate the transdermal administration of microneedles across BBB, the transport mechanism was validated by a transdermal model to restore the in vivo transport behavior of the Rh-NPs-DMNs administration mode. The results of the in vitro dissolution test Rh-NPs-DMNs (Figure 5) inserted into the isolated skin revealed that the microneedle tip slowly dissolved within 0–30 s and the microneedle was dissolved to approximately 60% of the initial length after 60 s. Moreover, the backing layer also gradually started to dissolve, and the reason for this was related to the hydrophilicity of HA and the gradually increasing pyramidal shape of the cross-sectional area of the microneedle tip from the backing. When dissolved for 10 min, the tip dissolution length was close to 100%, demonstrating that the physical promotion of permeation by microneedle can release NPs into the formed micro-pore channels in a short period.

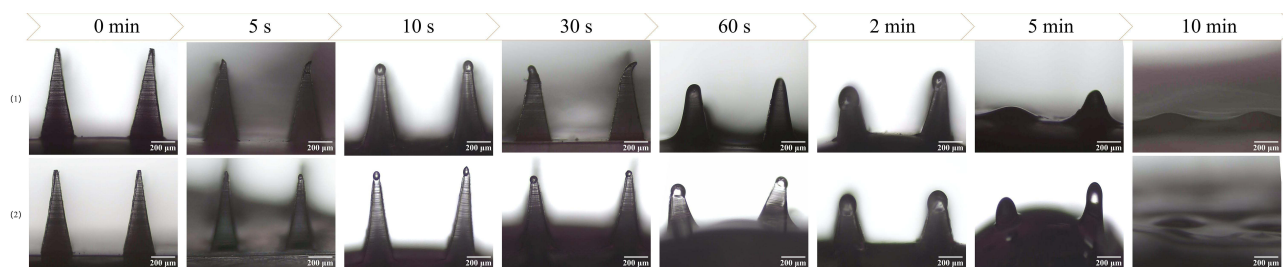


Figure 5 Morphological changes within 10 min of microneedle puncture into isolated rat abdominal skin. (4×, Scale bars = 200 μm)(1: Rh-NPs-DMNs; 2: Rh-DMNs).

Tissue cry sectioning experiments showed that the fluorescence intensity and distribution of Rh-NPs-DMNs in the skin layer gradually increased as the administration time of Rh-NPs-DMNs increased (Figure 6A). After 10 min of administration in the Rh-NPs-DMNs group, fluorescence accumulation deep in the skin was noted, and this depth signified the penetration depth of the needle tip (approximately 400 μm), denoting quick and effective delivery of NPs across the stratum corneum barrier by microneedle administration. The microneedles slowly dissolve over time through the action of the skin matrix solution, letting the drug be released and gradually spread deeper into the skin with time-dependent fluorescence intensity. At about 1000 μm of dermal tissue, the Rh-NPs-DMNs group showed a deeper distribution of fluorescence intensity than the Rh-DMNs group when the 12-h period was reached. This finding further proposes that NPs are more conducive to entering the skin through microcirculation or mucosal contact to deliver the drug through blood vessels or lymphatic vessels.

The H&E staining findings of the skin tissue is shown in Figure 6B: immediately after Rh-NPs-DMNs administration, obvious micron-sized mechanical pore channels were observed, which measured approximately 80% of the tip length (approximately 550 μm); this length was sufficient to cross the stratum corneum barrier of approximately 70–1200 μm in thickness and still maintain the collagen fullness of the dermis and the tight structure of the fibrous layer. However, some microporous channels remained in the epidermis even after 12 h of microneedle administration. At this moment, the backing layer, a drug reservoir, can still diffuse into the dermis and consequently enter the body's circulation through capillaries to deliver the drug to the target site, maintain a stable blood concentration, and improve the bioavailability of the drug. After 24 h of microneedle administration, the overall skin returned to the same state as that of the blank group, with intact and neatly lined up cell structure and almost no inflammatory cells.

Visual observation of skin healing after drug administration revealed that the skin surface formed evident micro-pore channels immediately after drug administration. When the drug was administered for approximately 5 min, the puncture effect was about 100% (Figure 6C) and some of the pore channels could no longer be observed by the naked eye, indicating that the pore channels formed after microneedle administration are a dynamic healing process. After 15 min of drug administration, the peripheral drug administration traces had disappeared, and the skin was the same as that before drug administration, without obvious wounds, erythema, and folds.

Discussion

With the development of an aging population, the incidence of central nervous system (CNS) diseases including Alzheimer's disease, Parkinson's disease, multiple sclerosis, stroke, and brain tumors is increasing and has become the second most common type of disease threatening human life. These diseases are caused by a variety of complex ischemic, hemorrhagic, inflammatory, neurodegenerative, and developmental disorders, which are prevalent and poorly treated. However, the success of CNS drug development is very low, and one of the most important constraints is the difficulty of crossing the blood–brain barrier (BBB). Almost all large-molecule drugs, including peptides, recombinant proteins, monoclonal antibodies, and drugs based on RNA interference technology, and more than 98% of small-molecule drugs fail to cross the blood–brain barrier, which seriously hinders the effective clinical treatment of CNS diseases.³³ Therefore, CNS drugs need to be able to overcome the BBB and achieve adequate exposure in the CNS while having safety and efficacy, which is the key to successful CNS drug development. The brain barrier is a key factor affecting the efficacy of central nervous system drugs, so increasing drug distribution to the brain could improve efficacy for possible new approaches to the treatment of refractory depression.

In order to achieve drug delivery across the BBB, existing research mainly focuses on directly interfering with the physiological barrier function of the BBB to reduce the obstruction of the blood–brain barrier, such as opening tight junctions³⁴ and inhibiting efflux pumps;³⁵ or rationally designing and modifying drug molecules³⁶ to change the properties of drugs to make them cross the BBB more easily, such as designing drugs by simulating endogenous molecules, pre-drug design, lipidation modification, glycosylation modification; and also coupling drugs with carriers to build effective brain drug delivery systems, such as monoclonal antibody delivery systems and cell shuttle peptide delivery systems. In addition, the use of appropriate routes of drug delivery, including nasal administration and intrathecal injection, has improved the success rate of crossing the BBB. A Nanoscale brain-targeted drug delivery system is a new type of nano drug delivery system, which can target drugs

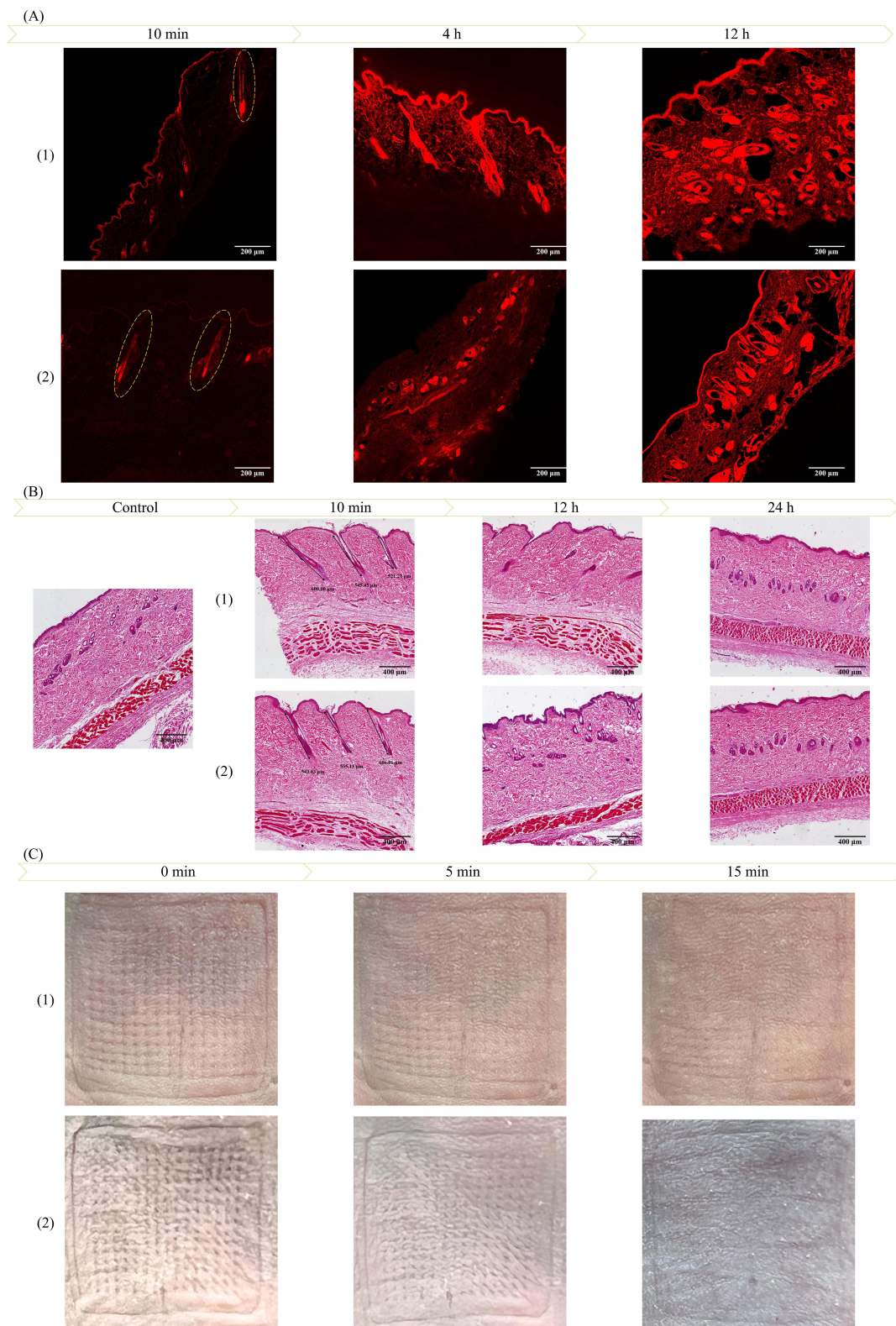


Figure 6 (A) Changes in fluorescence intensity and depth of skin at different time points (10×, Scale bars = 200 μm) and safety evaluation. (B) Tissue section results (5×, Scale bars = 400 μm); (C) Healing at the microneedle administration site; 1: Rh-NPs-DMNs; 2: Rh-DMNs).

specifically to diseased tissues, organs, and even cells, with the characteristics of low dosage, high efficacy, and low toxic side effects, and the drug delivery method and speed can be easily controlled.³⁷ However, for effective brain drug delivery, crossing the blood–brain barrier is only the first step, how the delivery system transports the drug within the brain to its target pathological site should also consider various mechanisms such as CNS solute clearance of nanoparticles, easy aggregation of nanocarriers, for example, liposomes remain confined to the stratum corneum in the skin,³⁸ and also because of their small size, they will remain in the distal part of the circulatory system and enter the nucleus to cause DNA damage,³⁹ which will affect the effectiveness and safety of the drug.

Therefore, in this study, the effect of transdermal administration of nanoparticles across the BBB into the CNS was investigated using microneedles as a vehicle, where NPs under 200 nm have a passive targeting effect, facilitating more drugs to be targeted for action in the brain.⁴⁰ In addition, the shortcomings of insufficient rigidity of NPs, poor self-deformability, and poor transfer efficiency due to biological barriers can be solved by combining DMNs with NPs in physical permeation-promoting methods,⁴¹ thus improving the permeation rate of drug transdermal absorption into the body.⁴² We used in vivo imaging techniques to dynamically observe the penetration behavior of Rh-NPs-DMNs and analyze the results of microneedle morphological changes in combination with H&E staining of isolated skin, frozen sections, and skin healing, respectively, to evaluate whether microneedle-loaded nanoparticles and/or APIs administered transdermally can achieve adequate exposure in the distal CNS. The results showed that the skin transfer of microneedle-loaded nanoparticles (Rh-NPs-DMNs) had stronger mechanical properties, deeper distribution of the drug in the skin tissue, and stronger fluorescence intensity than the API-loaded drug (Rh-DMNs). The research results can improve the precision of brain-targeted drug delivery systems and provide new ideas for the treatment of central nervous system diseases.

Conclusion

The skin is the largest organ in the human body and has been studied to deliver vaccines, hypoglycemic agents, genes, anesthetics, and antineoplastic drugs safely and stably through this route, and all of them can achieve good therapeutic effects. In this paper, PLGA nanoparticulate-based microneedle system (Rh-NPs-DMNs) was designed and developed for the treatment of central nervous system diseases. PLGA, which is biodegradable and has a large drug loading capacity, was used as a carrier and combined with microneedle technology for effective transdermal delivery, with the aim of reducing the clearance of large molecules by the mononuclear macrophage system while increasing the drug transport to the brain and prolonging the therapeutic activity of the drug in the body circulation. The permeation behavior of Rh-NPs-DMNs was vigorously observed using in vivo imaging technique and analyzed in combination with the results of H&E staining of isolated skin, frozen sections, skin healing, and other microneedle morphological changes; the findings revealed that the drug was continuously released in the interstitial fluid of the skin and entered the body circulation and reached the brain. The Rh-NPs-DMNs group showed a stronger fluorescent signal than the Rh-DMNs group (** $P < 0.01$); Rh-NPs-DMNs were also observed in the sub-tissue hippocampus with a relatively strong fluorescent signal ($*P < 0.05$) and had greater skin penetration. Therefore, NPs-laden Rh-DMNs can generate the potential for delivery across BBB to the brain, providing the basis for their need for clinical application across the blood–brain barrier.

Abbreviations

Rh, rhodamine-B; PLGA, poly(lactide-co-glycolide); NPs, nanoparticles; DMNs, dissolving microneedles; HA, hyaluronic acid; 2-HP- β -CD, 2-hydroxypropyl- β -cyclodextrin; PVA, polyvinyl alcohol; $N_{\text{eff}}\%$, needle tip-forming effect; $P_{\text{eff}}\%$, penetration efficiency; H&E, hematoxylin–eosin; SD rats, Sprague–Dawley rats; SM, stereo microscope; PM, polarizing microscope; SEM, Scanning electron microscopy; TEM, transmission electron microscopy.

Data Sharing Statement

The data that support the findings of this study are available from the corresponding author upon reasonable request.

Ethics Approval and Informed Consent

The study was approved by the Institutional Animal Care and Use Committee of Guangdong Pharmaceutical University (gdpulac 2023005), which ensures that the procedures employed meet guidelines for the care and use of laboratory animals. Sprague-Dawley rats were used in the experiment. The Guangdong Medical Animal Experimental Center provided the animals. Moreover, approval was received before beginning this research.

Consent for Publication

The authors declare that they have no known competing financial interests or personal relationships that could have appeared to influence the work reported in this paper.

Author Contributions

All authors made a significant contribution to the work reported, whether that is in the conception, study design, execution, acquisition of data, analysis, and interpretation, or all these areas; took part in drafting, revising, or critically reviewing the article; gave final approval of the version to be published; have agreed on the journal to which the article has been submitted; and agree to be accountable for all aspects of the work.

Funding

This work was supported by the Guangdong Administration Traditional Chinese Medicine (Grant Number: 20232120); the Innovation and Entrepreneurship Training Program for College Students (Grant Number: 202210573023); Guangdong Science and Technology Innovation Strategy Special Fund (Student Science and Technology Innovation Cultivation) Project (Grant Number: pdjh2023b0275).

Disclosure

The authors declare that they have no conflicts of interest in this work.

References

1. Gorick CM, Breza VR, Nowak KM, et al. Applications of focused ultrasound-mediated blood-brain barrier opening. *Adv Drug Deliv Rev.* 2022;191:114583. doi:10.1016/j.addr.2022.114583
2. Wang J, Li Z, Pan M, et al. Ultrasound-mediated blood-brain barrier opening: an effective drug delivery system for theranostics of brain diseases. *Adv Drug Deliv Rev.* 2022;190:114539.
3. Meng Y, Goubran M, Rabin JS, et al. Blood-brain barrier opening of the default mode network in Alzheimer's disease with magnetic resonance-guided focused ultrasound. *Brain.* 2023;146(3):865–872.
4. Lei S, Li J, Yu J, et al. Porphyromonas gingivalis bacteremia increases the permeability of the blood-brain barrier via the Mfsd2a/Caveolin-1 mediated transcytosis pathway. *Int J Oral Sci.* 2023;15(1):3.
5. Anwar MM, Özkan E, Shomalizadeh N, et al. Assessing the role of primary healthy microglia and gap junction blocker in hindering Alzheimer's disease neuroinflammatory type: early approaches for therapeutic intervention. *Front Neurosci.* 2023;16:546.
6. Gernert M, Feja M. Bypassing the blood-brain barrier: direct intracranial drug delivery in epilepsies. *Pharmaceutics.* 2020;12(12):1134.
7. Kang JH, Ko YT. Intraosseous administration into the skull: potential blood-brain barrier bypassing route for brain drug delivery. *Bioeng Translational Med.* 2022;e10424.
8. Liu Y, Hong H, Xue J, et al. Near-infrared radiation-assisted drug delivery nanoplatfom to realize blood-brain barrier crossing and protection for parkinsonian therapy. *ACS Appl Mater Interfaces.* 2021;13(31):37746–37760.
9. Pena ES, Graham-Gurysh EG, Bachelder EM, Ainslie KM. Design of biopolymer-based interstitial therapies for the treatment of glioblastoma. *Int J Mol Sci.* 2021;22(23):13160.
10. Reshma S, Megha KB, Amir S, Rukhiya S, Mohanan PV. Blood brain barrier-on-A-chip to model neurological diseases. *J Drug Deliv Sci Technol.* 2023;80:104174.
11. Wei F, Wang Q, Liu H, et al. High Efficacy Combined Microneedles Array with Methotrexate Nanocrystals for Effective Anti-Rheumatoid Arthritis. *Int J Nanomedicine.* 2022;17:2397–2412.
12. Wu X, Huang D, Xu Y, Chen G, Zhao Y. Microfluidic templated stem cell spheroid microneedles for diabetic wound treatment. *Adv Mater.* 2014;1:2301064.
13. Chen H, Fan L, Peng N, et al. Galunisertib-loaded gelatin methacryloyl hydrogel microneedle patch for cardiac repair after myocardial infarction. *ACS Appl Mater Interfaces.* 2022;14(36):40491–40500.
14. Zhang Y, Ye F, Zhang T, et al. Structural basis of ketamine action on human NMDA receptors. *Nature.* 2021;596(7871):301–305.
15. Courtenay AJ, McAlister E, McCrudden MTC, et al. Hydrogel-forming microneedle arrays as a therapeutic option for transdermal esketamine delivery. *J Controlled Release.* 2020;322:177–186.

16. Pervaiz F, Saba A, Yasin H, et al. Fabrication of solid lipid nanoparticles-based patches of paroxetine and their ex-vivo permeation behaviour. *Artif Cells Nanomed Biotechnol.* 2023;51(1):108–119.
17. Kowalska M, Nowaczyk J, Fijałkowski Ł, Nowaczyk A. Paroxetine—overview of the molecular mechanisms of action. *Int J Mol Sci.* 2021;22(4):1662.
18. Li F, Wen Y, Zhang Y, et al. Characterisation of 2-HP-beta-cyclodextrin-PLGA nanoparticle complexes for potential use as ocular drug delivery vehicles. *Artif Cells Nanomed Biotechnol.* 2019;47(1):4097–4108.
19. Men Z, Lu X, He T, Wu M, Su T, Shen T. Microneedle patch-assisted transdermal administration of recombinant hirudin for the treatment of thrombotic diseases. *Int J Pharm.* 2022;612:121332.
20. Zhang W, Mehta A, Tong Z, Esser L, Voelcker NH. Development of polymeric nanoparticles for blood–brain barrier transfer—strategies and challenges. *Adv Sci.* 2021;8(10):2003937.
21. López-Cabeza R, Kah M, Grillo R, Bilková Z, Hofman J. Is centrifugal ultrafiltration a robust method for determining encapsulation efficiency of pesticide nanoformulations? *Nanoscale.* 2021;13(10):5410–5418.
22. Ghazi RF, Al-Mayahy MH. Levothyroxine sodium loaded dissolving microneedle arrays for transdermal delivery. *ADMET and DMPK.* 2022;10(3):213–230.
23. Li H, Yao J, Guo Y, et al. Preparation of conotoxin-encapsulated chitosan nanoparticles and evaluation of their skin permeability. *AAPS PharmSciTech.* 2023;24(1):53.
24. Hawkins S, Dasgupta BR, Ananthapadmanabhan KP. Role of pH in skin cleansing. *Int J Cosmet Sci.* 2021;43(4):474–483.
25. Min HS, Kim Y, Nam J, et al. Shape of dissolving microneedles determines skin penetration ability and efficacy of drug delivery. *Biomaterials Adv.* 2023;145:213248.
26. Han X, Ma T, Wang Q, et al. The mechanism of oxymatrine on atopic dermatitis in mice based on SOCS1/JAK-STAT3 pathway. *Front Pharmacol.* 2023;13.
27. Kucharz K, Kristensen K, Johnsen KB, et al. Post-capillary venules are the key locus for transcytosis-mediated brain delivery of therapeutic nanoparticles. *Nat Commun.* 2021;12(1):4121.
28. Xiang H, Xu S, Zhang W, Li Y, Zhou Y, Miao X. Skin permeation of curcumin nanocrystals: effect of particle size, delivery vehicles, and permeation enhancer. *Colloids Surf B Biointerfaces.* 2023;224:113203.
29. Chi Y, Huang Y, Kang Y, et al. The effects of molecular weight of hyaluronic acid on transdermal delivery efficiencies of dissolving microneedles. *Eur J Pharmaceutical Sci.* 2022;168:106075.
30. Bognanni N, Viale M, La Piana L, et al. Hyaluronan-cyclodextrin conjugates as doxorubicin delivery systems. *Pharmaceutics.* 2023;15(2):374.
31. Kang MS, Kwon M, Lee SH, et al. 3D printing of skin equivalents with hair follicle structures and epidermal-papillary-dermal layers using gelatin/hyaluronic acid hydrogels. *Chemistry Asian J.* 2022;17(18):e202200620.
32. Wang H, Mu X, Yang J, Liang Y, Zhang X-D, Ming D. Brain imaging with near-infrared fluorophores. *Coord Chem Rev.* 2019;380:550–571.
33. Malong L, Napoli I, Casal G, et al. Characterization of the structure and control of the blood-nerve barrier identifies avenues for therapeutic delivery. *Dev Cell.* 2023;58(3):174–191.e178.
34. Semyachkina-Glushkovskaya O, Bragin D, Bragina O, et al. Low-level laser treatment induces the blood-brain barrier opening and the brain drainage system activation: delivery of liposomes into mouse glioblastoma. *Pharmaceutics.* 2023;15(2):567.
35. Lin J-F, Liu Y-S, Huang Y-C, et al. Borneol and Tetrandrine Modulate the Blood–Brain Barrier and Blood–Tumor Barrier to Improve the Therapeutic Efficacy of 5-Fluorouracil in Brain Metastasis. *Integr Cancer Ther.* 2022;21:15347354221077682.
36. Sahu KJ, Mishra KA. Tools in the Design of Therapeutic Drugs for CNS Disorders: an up-to-date Review. *Curr Mol Pharmacol.* 2018;11(4):270–278.
37. Liu T, Xie Q, Dong Z, Peng Q. Nanoparticles-based delivery system and its potentials in treating central nervous system disorders. *Nanotechnology.* 2022;33(45):452001.
38. Bellefroid C, Lechanteur A, Evrard B, Mottet D, Debacq-Chainiaux F, Piel G. In vitro skin penetration enhancement techniques: a combined approach of ethosomes and microneedles. *Int J Pharm.* 2019;572:118793.
39. Rawat M, Singh D, Saraf S, Saraf S. Nanocarriers: promising vehicle for bioactive drugs. *Biol Pharm Bull.* 2006;29(9):1790–1798.
40. Meng Q, Meng H, Pan Y, et al. Influence of nanoparticle size on blood–brain barrier penetration and the accumulation of anti-seizure medicines in the brain. *J Materials Chem B.* 2022;10(2):271–281.
41. Ruan S, Zhang Y, Feng N. Microneedle-mediated transdermal nanodelivery systems: a review. *Biomaterials Sci.* 2021;9(24):8065–8089.
42. Prabakar K, Udhumansa U, Elsherbiny N, Qushawy M. Microneedle mediated transdermal delivery of β -sitosterol loaded nanostructured lipid nanoparticles for androgenic alopecia. *Drug Deliv.* 2022;29(1):3022–3034.

International Journal of Nanomedicine

Dovepress

Publish your work in this journal

The International Journal of Nanomedicine is an international, peer-reviewed journal focusing on the application of nanotechnology in diagnostics, therapeutics, and drug delivery systems throughout the biomedical field. This journal is indexed on PubMed Central, MedLine, CAS, SciSearch®, Current Contents®/Clinical Medicine, Journal Citation Reports/Science Edition, EMBASE, Scopus and the Elsevier Bibliographic databases. The manuscript management system is completely online and includes a very quick and fair peer-review system, which is all easy to use. Visit <http://www.dovepress.com/testimonials.php> to read real quotes from published authors.

Submit your manuscript here: <https://www.dovepress.com/international-journal-of-nanomedicine-journal>